Physics – Uspekhi **67** (11) 1111 – 1118 (2024)

REVIEWS OF TOPICAL PROBLEMS

PACS numbers: **71.70. – d,** 78.20.Bh, 78.40.Ha, 78.55.Hx, **78.90. + t**

55th ANNIVERSARY OF THE INSTITUTE OF SPECTROSCOPY
OF THE RUSSIAN ACADEMY OF SCIENCES (ISAN)

High-resolution spectroscopy of functional dielectrics with rare-earth ions

M N Popova, M Diab, K N Boldyrev

DOI: https://doi.org/10.3367/UFNe.2024.07.039714

Contents

Abstract. A brief review of recent studies of crystals doped with rare-earth ions performed at the Institute of Spectroscopy of the Russian Academy of Sciences (ISAN) using high-resolution wide-range optical Fourier spectroscopy is presented. The results of a study of inhomogeneous broadening and the fine structure of lines in the absorption and luminescence spectra of crystals with rare-earth ions caused by random deformations, the isotopic structure in luminescence spectra associated with matrix isotopes, and anticrossings of the crystal hyperfine levels in a magnetic field are discussed. It is shown that the hyperfine structure in luminescence spectra can be used to implement a luminescence thermometer for the region of ultra-low temperatures.

Keywords: spectra of crystals with rare-earth ions, deformation splittings, hyperfine structure, level anticrossings, photoluminescence, high-resolution Fourier spectroscopy, luminescence cryothermometer

1. Introduction

Since its foundation in 1968, the Institute of Spectroscopy of the Russian Academy of Sciences (ISAN) has made consistent efforts to master and develop the method of high-resolution Fourier spectroscopy. The founder and first director of ISAN, Sergei Leonidovich Mandelstam, while still head of the Spectroscopy Laboratory at the Lebedev Physical Institute, initiated work on creating the first Soviet high-resolution Fourier spectrometer in 1958. At that time, achievements in this area were only at the Aimé Cotton Laboratory in France (Pierre Jacquinot, Pierre and Janine Connes). As a result of joint work carried out at the Lebedev Physical Institute, the Commission on Spectroscopy, ISAN, and the Central Design Bureau of Unique Instrumentation of the Academy of Sciences of the USSR, the unique high-resolution infrared Fourier spectrometers (0.005 cm^{-1}) UFS-01 (1968) [1] and UFS-02 (1984) [2, 3] were designed, manufactured, and installed at ISAN.

Fourier spectroscopy has a number of advantages over scanning devices. The well-known advantages are: the multiplex (Fellgett's) advantage, the aperture ratio (Jacquinot's) advantage, and the wavenumber accuracy (Connes's) advantage [4]. Unlike the Fabry–Pérot interferometer, a modern Fourier spectrometer has a virtually unlimited free dispersion region. At the same time, frequency reference in the entire spectral region is carried out using a well frequency-stabilized laser, which eliminates the problems associated with frequency calibration that arise in laser spectroscopy. All these advantages are fully realized when recording extended spectra rich in narrow lines. These are the spectra of atoms, molecules, and rare-earth (RE) ions in crystals. In solid-state research, high-resolution spectroscopy is in demand in the study of materials for quantum information technology devices, sensors, photonics, and photovoltaic devices. It offers new possibilities in the study of phase transitions of various nature and the search for and study of new materials and new phenomena.

At ISAN, wide-range high-resolution Fourier spectroscopy is used to study the electron and phonon spectra of

M N Popova [1, a], **M Diab** [1, 2, b], **K N Boldyrev** [1, c]
[1] Institute of Spectroscopy, Russian Academy of Sciences, ul. Fizicheskaya 5, 108840 Troitsk, Moscow, Russian Federation
[2] Moscow Institute of Physics and Technology (National Research University), Institutskii per. 9, 141701 Dolgoprudnyi, Moscow region, Russian Federation
E-mail: [a] popova@isan.troitsk.ru, [b] diab.m@phystech.edu, [c] kn.boldyrev@gmail.com

Received 11 March 2024, revised 3 July 2024
Uspekhi Fizicheskikh Nauk **194** (11) 1177 – 1184 (2024)
Translated by V L Derbov

crystals with rare-earth ions and ions of transition metals, including magnetic ones, hybrid perovskites, and diamonds with color centers. The research is carried out in collaboration with theoreticians (mainly, B Z Malkin's team at Kazan Federal University). In this article, we will focus on recent studies of dielectrics with rare-earth ions. Crystals doped with rare-earth elements have a very small homogeneous and inhomogeneous linewidth of $4f^n - 4f^n$ optical transitions, since the $4f^n$ electron shell is well shielded from the influence of the crystalline environment by filled 5s and 5p shells. Narrow spectral lines allow probing the environment of a rare-earth ion in a crystal, obtaining information about defects, and studying subtle physical effects in crystals. $4f^n - 4f^n$ transitions cover the entire visible and infrared ranges, and the method of wide-range high-resolution Fourier spectroscopy is adequate for their study.

This article provides a brief overview of recent results on the study of inhomogeneous broadening and the fine structure of spectral lines caused by random deformations in a crystal, effects in luminescence spectra caused by isotopic disorder in the crystal lattice, and hyperfine interactions for a crystal in a magnetic field. The first results on the temperature dependences of the hyperfine structure (HFS) in luminescence spectra are also presented, which can form the basis for the creation of luminescence thermometers for remote measurement of ultra-low temperatures. We use a unique experimental facility of ISAN; more details about it are presented in the next section.

2. Research methods

All experimental results were obtained using a unique research facility (URF), which has no analogues in the world, created in the Laboratory of Fourier Spectroscopy of ISAN on the basis of the Bruker IFS125HR [5] high-resolution Fourier spectrometer. Recently, large-scale research and development work has been carried out to upgrade the URF. The facility makes it possible to record absorption/reflection/polarimetry/luminescence spectra in the terahertz, infrared, visible, and ultraviolet ranges (10–50,000 cm^{-1}) in the temperature range of 1.5 K (pumping out helium vapor)–650 K with a resolution of up to 0.0006 cm^{-1} (18 MHz). A modern silicon photomultiplier (SiPM) with low dark noise allows recording very weak signals (Raman scattering, photoluminescence). In the terahertz region, helium bolometers are used as detectors. The Sumitomo SHI SRP092 closed-loop cryostat is designed to conduct optical experiments at temperatures as small as 2.5 K in a magnetic field of up to 1.2 T. The vacuum three-axis adaptation of the bellows-type allows for the high-precision orientation of the cryostat in the optical beam.

3. Deformation fine structure of spectral lines

Real crystals always contain defects, either intrinsic or due to specially introduced impurities. These defects, in addition to local perturbation of the lattice structure, induce long-range internal deformation fields. Random deformations significantly change the magnetic, dielectric, elastic, and optical properties of crystals. In particular, they affect the processes that violate coherence in quantum information technology devices [6]. In the spectra of crystals, lattice defects cause inhomogeneous broadening. Inhomogeneous broadening has been studied in detail experimentally and theoretically for

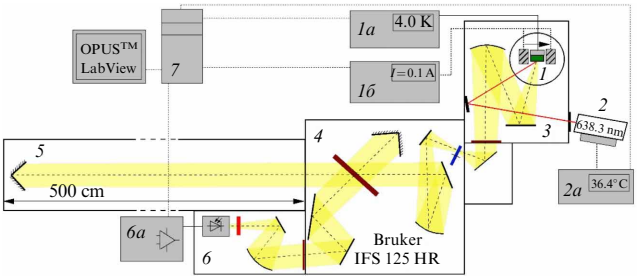

Figure 1. Setup: *1* — cryostat with electromagnet (hatched on gray background), *1a* — temperature controller, *1b* — power supply for electromagnet; *2* — temperature stabilized diode laser, *2a* — temperature controller and power supply for laser; *3* — fluorescence unit; *4–5* — Fourier spectrometer with moving mirror *5*; *6* — luminescence registration unit, *6a* — preamplifier and analog-to-digital converter; *7* — workstation for calculating spectra and automatic control of magnetic field and temperature.

transitions between nondegenerate levels of impurity centers [7–9]. In the fundamental study by Stoneham [10], a statistical theory of the shape of an inhomogeneously broadened zero-phonon line of a singlet-singlet transition in an activator center of a crystal with a low defect concentration was constructed in the elastic continuum approximation. In the case of a non-Kramers degenerate energy level, deformations that lower the symmetry of the center split the level. As a result, in particular, a doublet was observed in the spectrum of the $CsCdBr_3 : Pr^{3+}$ crystal instead of a hyperfine structure of six components [11]. Interestingly, improvements in growth technology made it possible to obtain a crystal in the spectrum of which a well-resolved HFS appeared. The increased central interval of the HFS indicated small residual deformations [12]. Such an increased central interval of the HFS was later observed in the spectra of scheelite $CaWO_4 : Ho^{3+}$ [13].

We have carried out a systematic study of the line shapes of transitions involving degenerate levels in impurity RE centers of different symmetries for non-Kramers and Kramers RE ions in crystals. The deformation fine structure (doublet, triplet) was observed in high-resolution optical spectra of RE-activated crystals with scheelite [14, 15], elpasolite [16], and zircon [17] structures. Figure 2 shows a line in the absorption spectrum of an $LiLuF_4 : Pr^{3+}$ crystal [18] corresponding to the transition from the ground singlet state to an excited doublet. As in the above-mentioned case of the spectrum of the $CsCdBr_3 : Pr^{3+}$ crystal, a doublet is observed instead of a hyperfine structure of six components.

Our colleagues from the Kazan Federal University (B Z Malkin's team) constructed a distribution function of random deformations induced by point defects in an elastically anisotropic continuum and developed a method for modeling the shape of spectral lines [15, 17]. The results of modeling one of the lines together with the experimental data are shown in Fig. 2. In recent papers [18, 19], deformation splittings in the spectra of pseudocubic perovskite $LaAlO_3$ doped with Ho^{3+} [18] or Tm^{3+} [19] ions were studied. A special feature of this crystal is the presence of twin domains, the boundaries of which serve as an additional source of random deformations. The recent observation of deformation splittings in luminescence spectra [19] opens the way to the creation of remote luminescence deformation sensors.

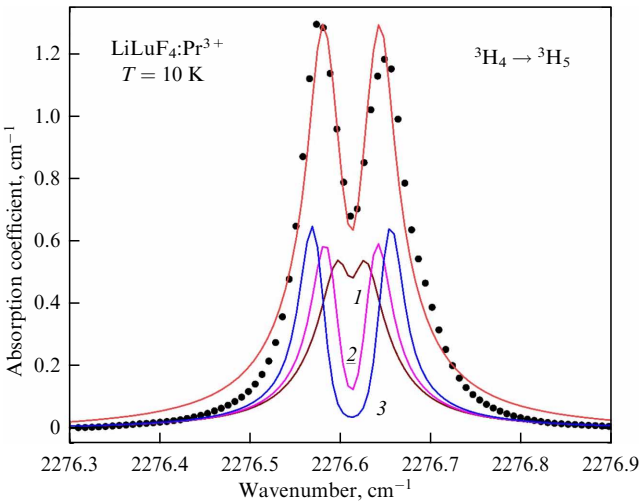

Figure 2. Line shape (dots — experiment, solid lines — calculation) corresponding to transitions in σ-polarization ($\mathbf{k} \perp c$, $\mathbf{E} \perp c$, $\mathbf{H} \| c$) of Pr^{3+} ions from singlet ground state $\Gamma_2(^3H_4)$ to excited doublet $\Gamma_{34}(^3H_5)$ in $LiLuF_4:Pr^{3+}$ crystal. $T = 10$ K. Lines *1*, *2*, and *3* are spectral envelopes of transitions between electron-nuclear states with nuclear spin projections $|m| = 1/2$, $3/2$, and $5/2$, respectively [15].

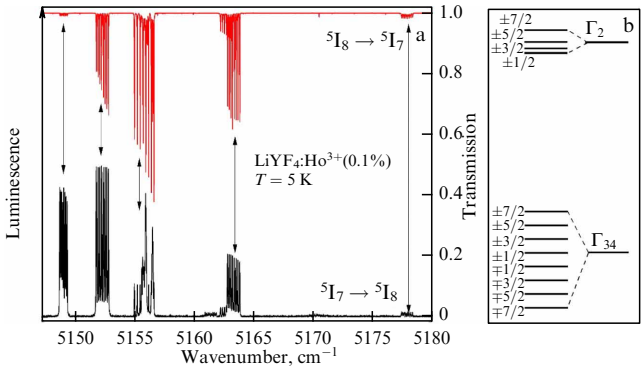

Figure 3. (a) Absorption (top red) and luminescence (bottom black, $\lambda_{excit} = 638.3$ nm) spectra in the region of transition between ground $^5I_8$ and excited $^5I_7$ multiplets of Ho^{3+} ion in $LiYF_4:Ho^{3+}$ (0.1 at.%) crystal at a temperature of 5 K. (b) Schematic diagram explaining HFS of doublet Γ_{34} and singlet Γ_1 or Γ_2 electron levels of Ho^{3+} ion. In the absence of a magnetic field, hyperfine sublevels are degenerate with respect to nuclear spin projections $\pm m$ (indicated on left).

4. High-resolution spectroscopy of $LiYF_4:Ho^{3+}$ crystals

Crystals of double lithium-yttrium fluoride with a scheelite structure doped with rare earth ions, $LiYF_4:RE^{3+}$, are used as active media for multi-frequency lasers [20–23] and master oscillators of high-power laser systems [24]; they are also considered for applications in modern quantum technology devices, such as quantum memory and quantum sensors [25–32]. It should also be noted that $LiYF_4:RE^{3+}$ crystals are known as model systems for studying various interactions and quantum phenomena [3, 33–45], which is facilitated by a record-low inhomogeneous broadening of the spectral lines of rare-earth ions in these crystals [26, 44].

4.1 Hyperfine and isotopic structure in luminescence spectra

Interest in the hyperfine structure in crystal spectra caused by the interaction of electrons with the magnetic dipole and electric quadrupole moments of the nucleus has recently revived due to the prospects of using the HFS in quantum technologies, in particular, for constructing Λ-systems for quantum memory [46, 47]. The HFS was previously studied in detail in absorption spectra (see, e.g., [3, 12, 14, 41, 48–53]). The HFS in luminescence spectra opens new possibilities, for example, for creating remote sensors. Recently, we were able to observe an HFS in the luminescence spectrum of a crystal for the first time [32, 54]. The HFS has been observed at many luminescent transitions in the $LiYF_4:Ho^{3+}$ crystal.

Figure 3a shows the spectral region of transitions in absorption (upper spectrum) and luminescence (lower spectrum) between the ground $^5I_8$ and the first excited $^5I_7$ multiplets of the Ho^{3+} ion. A well-resolved hyperfine structure of the lines is visible. The hyperfine structure of the absorption spectra of the $LiYF_4:Ho^{3+}$ crystal was studied in detail earlier [3, 41, 48, 49]. The wave functions of the crystal-field energy levels of the Ho^{3+} ion are transformed according to one-dimensional Γ_1 and Γ_2 and two-dimensional Γ_{34} irreducible representations of the S_4 point symmetry group of the position of holmium substituting for yttrium in $LiYF_4$. In a zero magnetic field, the Γ_{34} levels have an eight-component equidistant hyperfine structure arising from the interaction of the 4f electrons and the magnetic moment of the holmium nucleus with spin $I = 7/2$. Each hyperfine component is doubly degenerate: states $|\Gamma_3, m\rangle$ and $|\Gamma_4, -m\rangle$ have the same energy (here, m is the component of the nuclear moment I along the crystallographic axis c, $-7/2 \leqslant m \leqslant 7/2$) [3, 48]. For nondegenerate electron states Γ_1 and Γ_2, a magnetic hyperfine structure is forbidden in the first approximation. Electric quadrupole and pseudo-quadrupole (magnetic dipole in the second approximation) hyperfine interactions split singlets Γ_1 and Γ_2 into four nonequidistant hyperfine sublevels and lead to the nonequidistant hyperfine structure of levels Γ_{34} [41].

It should be noted that in $LiYF_4:Ho^{3+}$ luminescence is also observed at transitions between excited multiplets, which expands the scope of its application. Thus, luminescence at transitions $^5I_5 \rightarrow {}^5I_7$ and $^5F_5 \rightarrow {}^5I_6$ falls into the U and S ranges of optical fiber transparency, respectively, and can be used to create remote sensors. In the transition $^5I_6 \rightarrow {}^5I_7$, which cannot be studied in absorption, record-breaking narrow lines with a width at a half maximum of 0.002–0.003 cm^{-1} are observed.

Previously, a fine structure of hyperfine components was discovered in the absorption spectra of $LiYF_4:Ho^{3+}$ and it was shown that it is caused by isotopic disorder in the lithium sublattice [42, 45]. Due to the difference in the masses of lithium isotopes, the amplitudes of their zero-point vibrations differ, which leads to different equilibrium positions of the nearest fluorine ions (due to the anharmonicity of vibrations) and, thus, to the dependence of the crystal field for the Ho^{3+} ion on the isotopic composition of lithium in its immediate environment. The same fine structure of hyperfine components is also observed in the luminescence spectra: examples are given in Fig. 4. Isotopic disorder in the crystalline matrix also contributes to the inhomogeneous broadening of lines [26, 43, 44, 56].

4.2 Luminescence of $^7LiYF_4:Ho^{3+}$ crystals in a magnetic field. Remote magnetic field sensor

Doubly degenerate hyperfine levels are split in an external magnetic field B directed along the c-axis of the crystal by the value $g_{\|}\mu_B B$, where $\mu_B = 0.4669$ $cm^{-1}\,T^{-1}$ is the Bohr

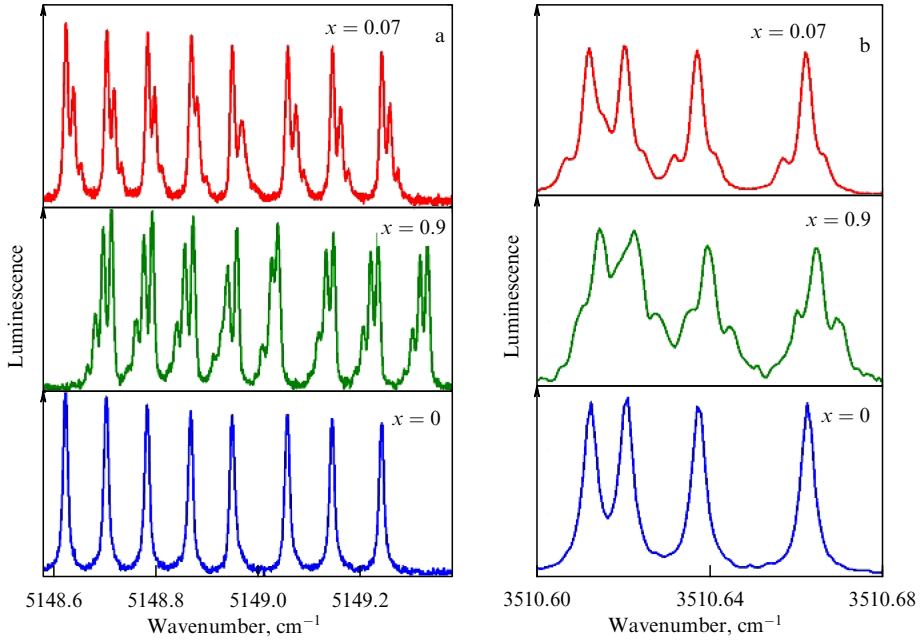

Figure 4. Isotopic structures in luminescence spectra of crystals $^{7}Li_{1-x}{}^{6}Li_{x}YF_4:Ho^{3+}$ (0.1 at.%) with $x = 0.07$ (natural lithium isotope content), $x = 0.9$ and $x = 0$. Regions of transitions (a) $^5I_7\Gamma_{34}(5155.75\ cm^{-1}) \rightarrow {}^5I_8\Gamma_2(6.85\ cm^{-1})$ and (b) $^5I_6\Gamma_1(8673.4\ cm^{-1}) \rightarrow {}^5I_7\Gamma_1(5162.8\ cm^{-1})$. $T = 6$ K, $\lambda_{excit} = 638.3$ nm.

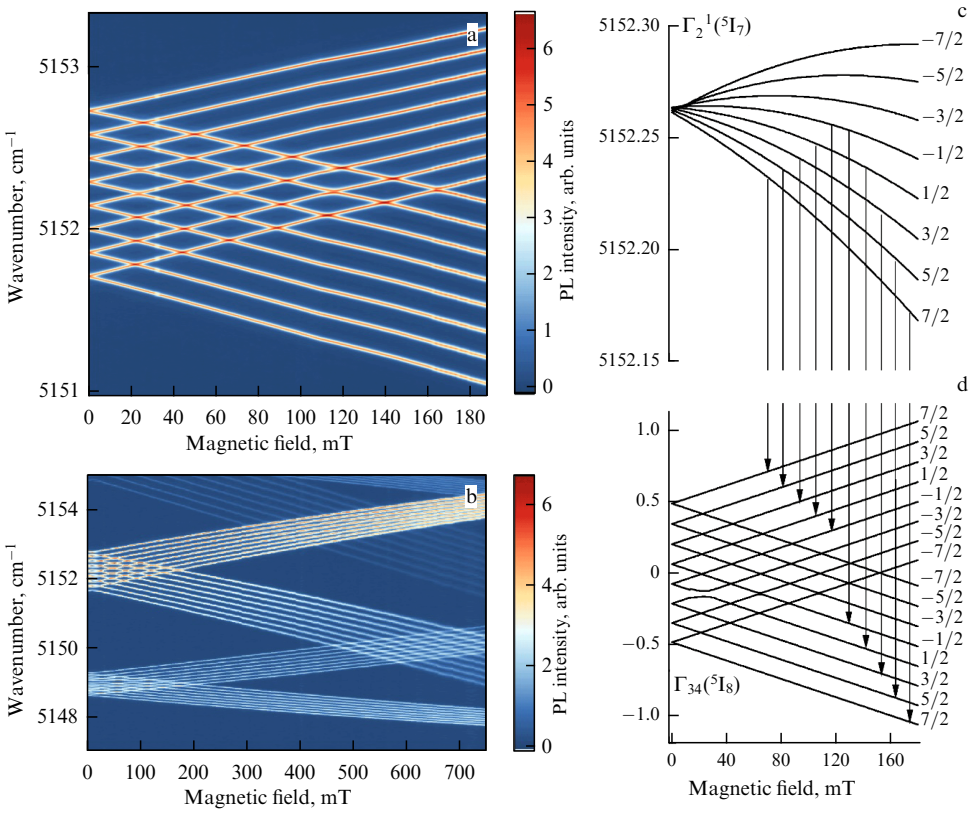

Figure 5. (a, b) Intensity maps of $LiYF_4:Ho^{3+}$ crystal luminescence ($T = 10$ K, $\lambda_{excit} = 638.3$ nm) in a magnetic field $\mathbf{B}||c$ (a) up to 180 mT in region of transition $^5I_7\Gamma_2(5152.3\ cm^{-1}) \rightarrow {}^5I_8\Gamma_{34}(0)$. Observed HFS and g-factor reflect corresponding parameters of the ground state: $\Delta_{HFS} = 0.148\ cm^{-1}$, $\langle g_{||}\rangle = 13.4$; (b) up to 700 mT. In addition to transition $^5I_7\Gamma_2(5152.3\ cm^{-1}) \rightarrow {}^5I_8\Gamma_{34}(0)$, transition $^5I_7\Gamma_{34}(5155.75\ cm^{-1}) \rightarrow {}^5I_8\Gamma_2(6.85\ cm^{-1})$ is shown, for which observed HFS and g-factor reflect corresponding parameters of excited state $^5I_7\Gamma_{34}(5155.75\ cm^{-1})$: $\Delta_{HFS} = 0.086\ cm^{-1}$, $\langle g_{||}\rangle = 6.1$. (c) Energies of hyperfine sublevels involved in $^5I_7\Gamma_2(5152.3\ cm^{-1}) \rightarrow {}^5I_8\Gamma_{34}(0)$ transition in $\mathbf{B}||c$ magnetic fields obtained by simulation [45]. Note the strongly differing energy scales for electron doublet and singlet. Black arrows show allowed transitions between hyperfine sublevels (to avoid overload, not all allowed transitions are shown).

magneton and $g_{||}$ is the g factor of the doublet. Note that the g factor is proportional to the hyperfine interval $\Delta_{\rm HFS}$: $|g_{||}| = 2g_0\Delta_{\rm HFS}/A_J$, where g_0 is the Lande factor and A_J is the magnetic hyperfine constant [3]. The intensity map in magnetic field–wavenumber coordinates in Fig. 5 for the luminescent transition from the lowest energy level of the $^5I_7$ multiplet (5152.3 cm^{-1}, Γ_2) to the ground level ($^5I_8$, 0 cm^{-1}, Γ_{34}) clearly shows how the HFS line behaves in a magnetic field $\mathbf{B}||c$. Since the initial level of the transition is a singlet, the observed HFS ($\Delta_{\rm HFS} = 0.148$ cm^{-1}) and g-factor ($g_{||} = 13.4$) reflect the corresponding parameters of the ground level. Luminescent transitions from singlets to the ground doublet, which has a large g-factor, can be used for remote sensing of the magnetic field. An even larger g-factor can be obtained for doublet-doublet transitions by adding up the g-factors of the levels participating in the transition. The line 6085.85 cm^{-1} is attractive, falling into the U-range of transparency of optical fibers. It corresponds to the transition $^5I_5\,\Gamma_{34}(11241.6) \rightarrow {}^5I_7\,\Gamma_{34}(5155.75)$ and is split according to the sum of the g-factors $g_{||}(11241.6) + g_{||}(5155.75) = 8.1 + 6.8 = 14.9$. Estimates show that it can be used to measure the magnitude of the magnetic field with an accuracy of $\delta B \approx 17$ μT [32] (for comparison, Earth's magnetic field is 30–50 μT, depending on latitude).

4.3 Anticrossings of hyperfine levels

Anticrossings play an important role in physics. This is a phenomenon when two eigenvalues of the Hamiltonian, depending on a continuous real parameter (for example, the magnetic field strength), cannot become equal in value ('intersect'). Anticrossings are induced by the interaction of different subsystems and are manifested in the appearance of a gap in the excitation spectrum of the system. Anticrossings are accompanied by the formation of coupled modes, energy renormalization, and the appearance of new branches in the excitation spectrum. An important example from solid state physics is the coupled states of an electromagnetic field and the excitations of the medium itself (excitons, phonons, plasmons) [57, 58]. Anticrossings caused by electron–phonon interactions have been observed in a variety of experiments using Raman scattering and infrared absorption and reflection [59–63], as well as neutron scattering [64]. The anticrossing effect due to the interaction of magnon and electron transitions between the crystal-field levels of rare-earth ions (Tb^{3+}) was observed in the far infrared region of the spectrum of garnet $Tb_3Fe_5O_{12}$ [65].

The first observation of hyperfine level anticrossings in the optical spectrum was reported in Refs [32, 45]. The phenomenon was observed in the absorption [45] and luminescence [32] spectra of $LiYF_4:Ho^{3+}$ crystals in a magnetic field. Examples of anticrossings are given in Fig. 6. Gaps from 0.01 to 0.06 cm^{-1} appear at points where hyperfine levels with nuclear spin projections differing by $|\Delta m| = 2$ and $|\Delta m| = 0$ converge.

Anticrossings $|\Delta m| = 2$ are due to the magnetic hyperfine interaction in the second order:

$$\Delta E_m^{m\pm2} = \left(\frac{A_J^2}{2}\right) \times \left\{ \frac{\left|\sum_k \langle \Gamma_{34}^+, m|\, J_+ I_-|\Gamma_2^k, m+1\rangle\langle\Gamma_2^k, m+1|\, J_+ I_-|\Gamma_{34}^-, m+2\rangle\right|}{E(\Gamma_2^k) - E(\Gamma_{34})} + \frac{\left|\sum_k \langle \Gamma_{34}^+, m|\, J_- I_+|\Gamma_1^k, m-1\rangle\langle\Gamma_1^k, m-1|\, J_- I_+|\Gamma_{34}^-, m-2\rangle\right|}{E(\Gamma_1^k) - E(\Gamma_{34})} \right\}. \quad (1)$$

The gap widths at the anticrossing points depend on the matrix elements of the operators J_+I_- and J_-I_+ and the

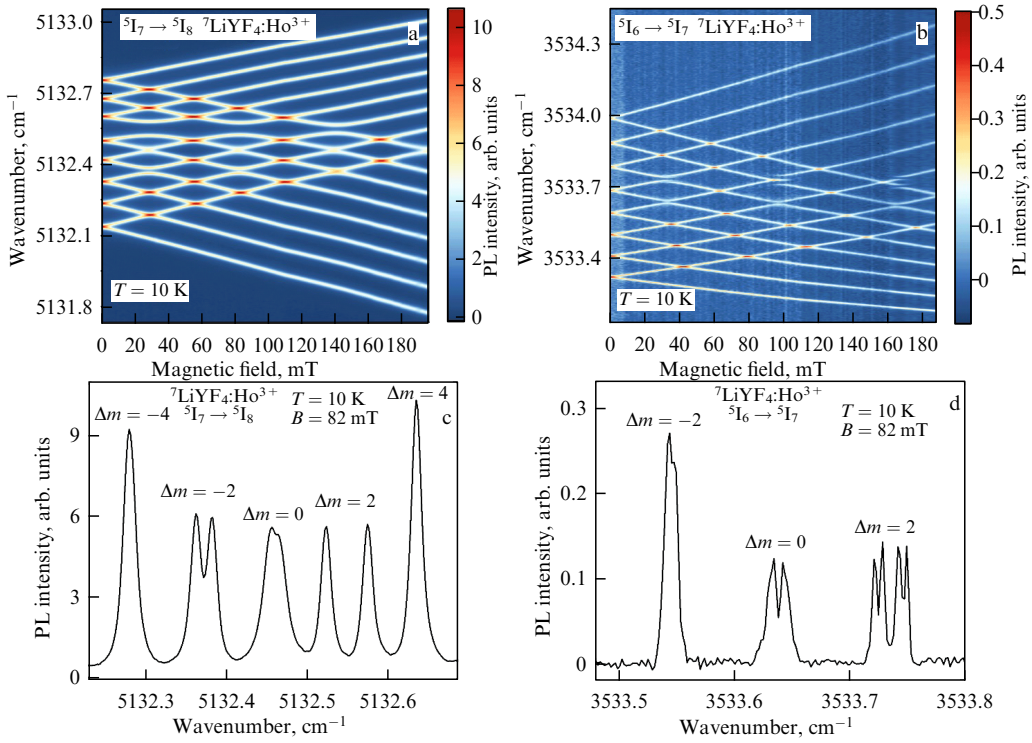

Figure 6. (a, b) Luminescence intensity maps for $LiYF_4:Ho^{3+}$ crystal in magnetic field $\mathbf{B}||c$ ($T = 10$ K, $\lambda_{\rm excit} = 638.3$ nm) for transitions (a) $^5I_7\Gamma_{34}(5155.75) \rightarrow {}^5I_8\Gamma_2(23.3)$ (line 5132.5) and (b) $^5I_6\Gamma_{34}(8685.9) \rightarrow {}^5I_7\Gamma_2(5152.3)$ (line 3533.6). (c, d) Fragments of spectra in regions of (c) third and (d) first crossings of hyperfine component.

energy separations between the given level Γ_{34} and the levels Γ_2 and Γ_1, respectively. In the case of the Γ_{34} levels 5155.75 cm^{-1} ($^5I_7$) and 8685.9 cm^{-1} ($^5I_6$), the luminescent transitions from which are shown in Fig. 6a, c and b, d, respectively, there are close levels of both Γ_2 and Γ_1 [32] and the gaps at anticrossings $\Delta m = 2$ and $\Delta m = -2$ are comparable in magnitude. At the anticrossing points and their vicinity, we have a superposition of wave functions of the form $a|\Gamma_{34}^{+}, m\rangle \pm b|\Gamma_{34}^{-}, m+2\rangle$. From such a superposition state, transitions to singlet levels with projections of the nuclear moment m and $m+2$ are allowed. If these levels are sufficiently separated (in a sufficiently strong magnetic field), then a four-component structure is observed [45], as in Fig. 6d.

The gaps observed at $\Delta m = 0$ crossings are of a different nature: they are caused by random lattice deformations always present in the crystal and reflect the quality of the crystal (see Section 3). By studying the anticrossings of hyperfine levels in a magnetic field, extremely small deformation splittings can be observed, which can be used to develop high-precision methods for crystal quality control.

5. Luminescence cryothermometry

In recent years, remote temperature measurement based on temperature-dependent luminescence characteristics (intensity, position and width of bands, decay times) has become widespread in such areas as chemical reactions, catalysis, microfluidics, micro- and nanoelectronics, photonics, and especially biology and medicine [66–68]. Color centers in diamonds, quantum dots in semiconductors, organic and hybrid phosphors, and micro- and nanocrystals of inorganic compounds containing rare-earth ions or transition metal ions are used as luminescence sources. The temperature range near room temperature and above, which is important for biology and chemistry, is well mastered in luminescence thermometry. However, for modern quantum technologies, aerospace research, and crystallographic measurements on a synchrotron, cryotemperature measurement is relevant.

In the low temperature region, the positions and widths of the luminescence lines change little, but their relative intensities can change significantly due to the redistribution of populations of levels close in energy. Therefore, the most adequate method for measuring cryotemperatures is Boltzmann ratiometric thermometry [69]. In this method, excited levels 1 and 2 are selected, separated in energy by the interval $\Delta E = E_2 - E_1$. Their equilibrium populations obey the Boltzmann distribution

$$\frac{n_2(T)}{n_1(T)} = \left(\frac{g_2}{g_1}\right) \exp\left(-\frac{\Delta E}{kT}\right),$$

where g_2 and g_1 are the degeneracy factors of levels 2 and 1, respectively, and k is the Boltzmann constant. The line intensity ratio (LIR) is measured for the luminescence from the selected levels:

$$\mathrm{LIR}(T) \equiv \frac{I_2(T)}{I_1(T)} = \frac{W_2 n_2(T)}{W_1 n_1(T)} = C \exp\left(-\frac{\Delta E}{kT}\right). \qquad (2)$$

Here, W_2 and W_1 are the probabilities of the involved transitions from levels 2 and 1, $C \equiv W_2 g_2 / W_1 g_1$. Formula (2) is valid if (i) the Boltzmann distribution is satisfied and (ii) the probabilities do not depend on temperature. Both of these conditions are not always satisfied [69], so, when constructing a Boltzmann ratiometric thermometer, it is necessary to compare the experimental values of $\mathrm{LIR}(T)$ with Eqn (2).

An important characteristic of a thermometer is its absolute sensitivity,

$$S_a(T) = \frac{dR(T)}{dT}, \qquad (3)$$

where $R(T)$ is the measured value. Relative sensitivity is used to compare thermometers based on different principles:

$$S_r(T) = \frac{1}{R}\frac{dR(T)}{dT}. \qquad (4)$$

In the case of a Boltzmann ratiometric thermometer, the absolute sensitivity $S_a(T)$ has a maximum at $T_m = \Delta E/2k$. The lower the measured temperatures (T_m), the closer the levels from which the luminescence lines are recorded should be chosen: $\Delta E \sim 2kT_m$. Obviously, the smaller the ΔE, the higher the spectral resolution required to record the spectra.

In a recent paper [70], we proposed pairs of luminescence lines of the $K_2YF_5:Er^{3+}$ crystal in the spectral region of the $^4I_{13/2} \rightarrow {}^4I_{15/2}$ transitions in the Er^{3+} ion (a region of about 1.5 μm, falling into the C-transparency window of an optical fiber) for the implementation of a Boltzmann luminescence ratiometric cryothermometer in the temperature range of about 20, 40, and 60 K. It was also shown that measuring the half-width of the luminescence line with a wavelength of 1.538 μm (6500 cm^{-1}) provides a simple and reliable way to record the temperature in the range from 20 to 90 K.

The idea of using the hyperfine structure seems attractive for measuring ultralow temperatures ($\leqslant 2$ K). We chose the 6089.3 cm^{-1} (1.642 μm) line in the luminescence spectrum of the $^7LiYF_4:Ho^{3+}$ crystal, corresponding to the transition $^5I_5\Gamma_{34}(11241.6) \rightarrow {}^5I_7\Gamma_2(5152.3)$ and falling into the U-transparency window of the optical fiber. It is shown in Fig. 7a for several temperatures. The initial level of the transition has an HFS with a record large interval of 0.178 cm^{-1}. The temperature dependence of the intensity ratio of the extreme frequency components of the HFS is shown in Fig. 7b together with the Boltzmann population ratio of the corresponding levels. It is evident that, at the temperatures accessible to us (not lower than 3 K), the Boltzmann population distribution of the hyperfine components of the level is fulfilled. Thus, the 1.642-μm line may be promising for constructing a Boltzmann luminescence ratiometric thermometer for temperatures of 0.5–5 K ($T_m = 0.9$ K).

6. Conclusion

Wide-range high-resolution Fourier spectroscopy has opened fundamentally new possibilities in solid-state research. The above results on the spectroscopy of crystals doped with rare-earth ions could not be obtained by any other method. The fine structure of lines in the absorption and luminescence spectra caused by random deformations of the crystal lattice was discovered and studied. Based on these experimental results, a statistical theory of inhomogeneous broadening of transition lines involving electronic doublets and triplets was constructed and a technique for modeling the shape of such lines was developed. These results can be used to assess the quality of crystals.

In the luminescence spectra of crystals, the hyperfine structure and isotopic structure caused by isotopic disorder in the matrix crystal were observed for the first time. A record

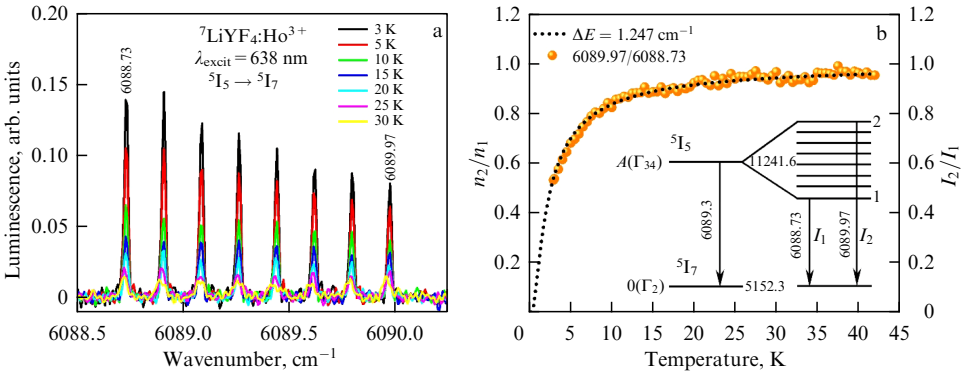

Figure 7. (a) Luminescence spectrum of ^{7}LiYF$_4$:Ho^{3+} crystal in region of transition ^{5}I$_5\Gamma_{34}$(11241.6) → ^{5}I$_7\Gamma_2$(5152.3) in Ho^{3+} ion; (b) temperature dependences of ratio I_2/I_1 of integral intensities of high-frequency and low-frequency hyperfine component of luminescence line 6089.3 cm^{-1} (1.642 μm) (transition ^{5}I$_5\Gamma_{34}$(11241.6) → ^{5}I$_7\Gamma_2$(5152.3)) (symbols), and population ratios n_2/n_1 of hyperfine levels 2 and 1, separated by an interval of 1.247 cm^{-1}, under the assumption of the Boltzmann distribution (dotted line).

narrow luminescence line with a width of 0.002 cm^{-1} at half-height was registered. These results were obtained on a LiYF$_4$:Ho^{3+} crystal. The splitting of luminescence lines of a monoisotopic ^{7}LiYF$_4$:Ho^{3+} crystal in an external magnetic field was studied. The possibility of creating a remote luminescence magnetic field sensor capable of ensuring measurement accuracy of the order of the magnitude of Earth's magnetic field was demonstrated.

For the first time, anticrossings of hyperfine levels in a magnetic field have been registered in optical spectra and investigated. It has been shown that gaps in the spectrum of the ^{7}LiYF$_4$:Ho^{3+} crystal at magnetic field values where levels with nuclear spin projection values differing by $|\Delta m| = 2$ should have crossed are due to magnetic hyperfine interaction in the second order, while anticrossings with $\Delta m = 0$ are a consequence of random deformations of the crystal lattice.

The results on the temperature dependence of the intensities of the hyperfine structure components of the ^{7}LiYF$_4$:Ho^{3+} luminescence line with a wavelength of about 1.642 μm (falling into the U-transparency window of the optical fiber) show the potential of this line for constructing a Boltzmann luminescence ratiometric cryothermometer.

The development of high-resolution spectroscopy methods at ISAN is largely due to the fruitful collaboration with B Z Malkin's theoretical group (Kazan Federal University). We are also grateful to all our co-authors of the papers [3, 12–19, 32, 41, 42, 45, 50, 51, 54–56, 62, 63, 70]. This work was supported by the Russian Science Foundation (RSF grant no. 19-72-10132). Section 5, "Luminescent cryothermometry," was written based on the results of the work within RSF project no. 23-12-00047.

References

1. Balashov A A et al. *Appl. Opt.* **17** 1716 (1978)
2. Agladze N I et al. *SPIE* **553** 452 (1985)
3. Agladze N I, Popova M N *Solid State Commun.* **55** 1097 (1985)
4. Efimova A I et al. *Sovremennaya Infrakrasnaya Spektroskopiya: Osnovy, Metody, Pribornaya Baza* (Modern Infrared Spectroscopy: Fundamentals, Methods, Instrumentation) (Moscow: Lan', 2023) Textbook for Universities; https://e.lanbook.com/book/319298
5. Unikal'naya nauchnaya ustanovka "Mnogofunktsional'naya shirokodiapazonnaya spektroskopiya vysokogo razresheniya" (UNU MShSVR) reg. nomer 508571, Institut spektroskopii RAN (Unique research facility "Multifunctional wide-range high-resolution spectroscopy" (URF MWRHRS) reg. No. 508571, Institute of Spectroscopy of the RAS), https://ckp-rf.ru/catalog/usu/508571/
6. Welinski S et al. *Opt. Mater.* **63** 69 (2017)
7. Freiberg A M, Rebane L A *Fiz. Tverd. Tela* **16** 2626 (1974)
8. Vasiliev A V, Logacheva E I, Ryskin A I *Izv. Akad. Nauk SSSR, Ser. Fiz.* **46** 300 (1982)
9. Kaplyanskii A A, Rozenbaum R B *Fiz. Tverd. Tela* **13** 2623 (1971)
10. Stoneham A M *Rev. Mod. Phys.* **41** 82 (1969)
11. Chaminade J P et al. *J. Luminescence* **48–49** 531 (1991)
12. Popova M N et al. *Phys. Rev. B* **63** 075103 (2001)
13. Shakurov G S et al. *Phys. Chem. Chem. Phys.* **16** 24727 (2014)
14. Klimin S A et al. *Phys. Rev. B* **81** 045113 (2010)
15. Abishev N M et al. *Phys. Solid State* **61** 795 (2019); *Fiz. Tverd. Tela* **61** 898 (2019)
16. Malkin B Z et al. *Phys. Rev. B* **86** 134110 (2012)
17. Malkin B Z et al. *Phys. Rev. B* **96** 014116 (2017)
18. Boldyrev K N et al. *Phys. Rev. B* **103** 054103 (2021)
19. Boldyrev K N et al. *Opt. Mater. X* **14** 100155 (2022)
20. Chicklis E P et al. *Appl. Phys. Lett.* **19** 119 (1971)
21. Gibert F et al. *Appl. Phys. B* **116** 967 (2014)
22. Wang Y et al. *Opt. Lett.* **44** 6049 (2019)
23. Luo S et al. *Opt. Commun.* **380** 357 (2016)
24. Strauss H J et al. *Opt. Express* **19** 13974 (2011)
25. Goldner P, Guillot-Noël O *Mol. Phys.* **102** 1185 (2004)
26. Thiel C W, Böttger T, Cone P L *J. Luminescence* **131** 353 (2011)
27. Akhmedzhanov R A et al. *Laser Phys. Lett.* **13** 115203 (2016)
28. Gerasimov K I et al. *Phys. Rev. B* **94** 054429 (2016)
29. Minnegaliev M M et al. *Quantum Electron.* **47** 778 (2017); *Kvantovaya Elektron.* **47** 778 (2017)
30. Kukharchyk N et al. *New J. Phys.* **20** 023044 (2018)
31. Akhmedzhanov R et al. *Phys. Rev. B* **97** 245123 (2018)
32. Boldyrev K N, Malkin B Z, Popova M N *Light Sci. Appl.* **11** 245 (2022)
33. Brooke J et al. *Science* **284** 779 (1999)
34. Giraud R et al. *Phys. Rev. Lett.* **87** 057203 (2001)
35. Ghosh S et al. *Science* **296** 2195 (2002)
36. Giraud R, Tkachuk A M, Barbara B *Phys. Rev. Lett.* **91** 257204 (2003)
37. Ghosh S et al. *Nature* **425** 48 (2003)
38. Rønnow H M et al. *Science* **308** 389 (2005)
39. Ancona-Torres C et al. *Phys. Rev. Lett.* **101** 057201 (2008)
40. Schmidt M A et al. *Proc. Natl. Acad. Sci. USA* **111** 3689 (2014)
41. Agladze N I, Vinogradov E A, Popova M N *Sov. Phys. JETP* **64** 716 (1986); *Zh. Eksp. Teor. Fiz.* **91** 1210 (1986)
42. Agladze N I et al. *Phys. Rev. Lett.* **66** 477 (1991)
43. Macfarlane R M, Cassanho A, Meltzer R S *Phys. Rev. Lett.* **69** 542 (1992)
44. Macfarlane R M, Meltzer R S, Malkin B Z *Phys. Rev. B* **58** 5692 (1998)
45. Boldyrev K N et al. *Phys. Rev. B* **99** 041105 (2019)
46. Goldner P, Ferrier A, Guillot-Noël O, in *Handbook on the Physics and Chemistry of Rare Earths* Vol. 46 (Eds J-C Bünzli, V K Pecharsky) (Amsterdam: Elsevier, 2015) p. 1, https://doi.org/10.1016/B978-0-444-63260-9.00267-4

47. Stuart J S et al. *Phys. Rev. Research* **3** L032054 (2021) https://doi.org/10.1103/PhysRevResearch.3.L032054
48. Matmon G et al. *Phys. Rev. B* **94** 205132 (2016)
49. Beckert A et al. *Phys. Rev. B* **106** 115119 (2022)
50. Boldyrev K N, Malkin B Z, Popova M N *J. Luminescence* **247** 118902 (2022)
51. Popova M N et al. *Phys. Rev. B* **61** 7421 (2000)
52. Baraldi A et al. *Phys. Rev. B* **76** 165130 (2007)
53. Mazzera M et al. *J. Phys. Condens. Matter* **24** 205501 (2012)
54. Boldyrev K N, Popova M N *J. Luminescence* **252** 119340 (2022)
55. Agladze N I et al. *J. Exp. Theor. Phys.* **77** 1021 (1993); *Zh. Eksp. Teor. Fiz.* **104** 4171 (1993)
56. Chukalina E P et al. *Phys. Lett. A* **269** 348 (2000)
57. Hopfield J J *Phys. Rev.* **112** 1555 (1958)
58. Agranovich V M, Ginzburg V L *Sov. Phys. Usp.* **5** 323 (1962); *Usp. Fiz. Nauk* **76** 643 (1962)
59. Dahl M, Schaack G *Phys. Rev. Lett.* **56** 232 (1986)
60. Kupchikov A K et al., in *Spektroskopiya Kristallov* (Spectroscopy of Crystals) (Exec. Ed. A A Kaplyanskii) (Leningrad: Nauka, 1989) p. 85
61. Brinzari T V et al. *Phys. Rev. Lett.* **111** 047202 (2013)
62. Boldyrev K N et al. *Phys. Rev. B* **90** 121101 (2014)
63. Boldyrev K N et al. *Phys. Rev. Lett.* **118** 167203 (2017)
64. Kjems J K, Hayes W, Smith S H *Phys. Rev. Lett.* **35** 1089 (1975)
65. Kang T D et al. *Phys. Rev. B* **82** 014414 (2010)
66. Marciniak L et al. *Coord. Chem. Rev.* **469** 214671 (2022)
67. Dramićanin M D *J. Appl. Phys.* **128** 040902 (2020)
68. Brites C D S, Balabhadra S, Carlos L D *Adv. Opt. Mater.* **7** 1801239 (2019)
69. Suta M, Meijerink A *Adv. Theory Simul.* **3** 2000176 (2020)
70. Boldyrev K N et al. *Opt. Spektrosk.* **131** 1335 (2023)